J. Fluid Mech. (1986), *vol.* 165, *pp.* 131–145
Printed in Great Britain

Hydrodynamic pressures on rigid dams during earthquakes

By PHILIP L.-F. LIU

Joseph H. DeFrees Hydraulics Laboratory, School of Civil and Environmental Engineering, Cornell University, Ithaca, NY 14853, USA

(Received 21 February 1985 and in revised form 20 August 1985)

The hydrodynamic pressures acting on the surface of a rigid dam during earthquakes are examined both analytically and numerically by a two-dimensional potential-flow theory. Analytical solutions are obtained for the cases where the inclined upstream dam face has a constant slope and the reservoir has a triangular shape. A general numerical scheme *via* an integral-equation formulation is also presented for complex geometries. Analytical and numerical solutions are compared with experimental data (Zangar 1953) with good agreement.

1. Introduction

Earthquake-induced hydrodynamic pressures on the upstream face of a dam are important factors in design considerations. Assuming that the fluid is incompressible, Westergaard (1933) was first to derive an expression for the hydrodynamic pressure acting on a rigid dam with a vertical upstream face as a result of horizontal harmonic ground motion. In the last fifty years, many researchers have extended Westergaard's classical work to include more physical parameters such as the compressibility of the fluid in the reservoir (e.g. Chopra 1967; Rashed & Iwan 1984), the flexibility of the dam (e.g. Finn & Varoglu 1973; Mei, Foda & Tong 1979), and reservoir bottom absorption (e.g. Fenves & Chopra 1983, 1985). Although there are many numerical models (e.g. Hall & Chopra 1982; Rashed 1982; Liu & Cheng 1984; Yeh & Ho 1984) that can be used for dam–reservoir-interaction problems with complex two- and three-dimensional geometries, analytical solutions are rare and are available only for a reservoir with a simple geometry.

Using a two-dimensional potential-flow theory, Chwang (1978) presented an analytical solution for the hydrodynamic pressure on an accelerating dam. The duration of the dam acceleration is short enough that the compressibility of the fluid can be ignored. The reservoir was assumed to have a constant depth and extend to infinity and the upstream dam face to have a constant slope. In a companion paper, Chwang & Housner (1978) solved the same problem approximately by the momentum-balance principle, which was first introduced by von Kármán (1933). Chwang (1979) extended the theory to a finite reservoir of triangular shape. The upstream dam face was assumed to be vertical. The effects of stratification in reservoirs on the hydrodynamic pressure were considered in Chwang (1981). These analytical solutions are of value in reaching a qualitative understanding of the hydrodynamic pressures on the dam.

The objectives of this paper are twofold. First, an analytical solution for the earthquake-acceleration-induced hydrodynamic pressure on a rigid sloping dam with a reservoir of triangular shape is presented. Both vertical and horizontal ground

motions are considered in the solution. Chwang's (1978, 1979) solutions become limiting cases of the present solution. Zangar's (1953) experimental data agree very well with analytical solutions for a reservoir of constant depth. The second objective of this paper is to present a numerical scheme to solve problems with complex geometries. The boundary-integral-equation method is chosen, since only the boundary information, i.e. hydrodynamic pressure on the dam face, is of interest. Numerical solutions are compared with Zangar's (1953) experimental results for several different geometries of dam face.

2. Theoretical formulation

Consider a rigid dam with an upstream face of an arbitrary shape (Γ_d in figure 1). The origin of the coordinates is located at the base of the dam and the free surface is represented by $y = h$. As shown in figure 1, the bottom of the reservoir is denoted as Γ_b. The dam-and-reservoir system is assumed to undergo a constant acceleration a_0 in the direction making an angle γ with the x-axis. Assuming that the fluid in the reservoir is incompressible and inviscid, the hydrodynamic pressure P satisfies the Laplace equation

$$\nabla^2 P = 0. \tag{1}$$

If the duration of the acceleration is sufficiently short, the free-surface perturbation is small and negligible. The only free-surface boundary condition is to require that the dynamic pressure vanish. Thus

$$P = 0 \quad (y = h). \tag{2}$$

Along the upstream dam face and the reservoir bottom the normal derivations of the dynamic pressure are prescribed:

$$\frac{\partial P}{\partial n_d} = -\rho \boldsymbol{a} \cdot \boldsymbol{n}_d \quad \text{on } \Gamma_d; \tag{3}$$

$$\frac{\partial P}{\partial n_b} = -\rho \boldsymbol{a} \cdot \boldsymbol{n}_b \quad \text{on } \Gamma_b; \tag{4}$$

where $\boldsymbol{a} = (a_0 \cos\gamma, a_0 \sin\gamma)$, and $\boldsymbol{n}_d$ and $\boldsymbol{n}_b$ are the unit outward normals along the dam surface and the reservoir respectively. In the case where the water depth is a constant, the reservoir becomes a semi-infinitely long channel. The hydrodynamic pressure vanishes as $x \to \infty$.

3. An analytical solution

3.1. *Analysis*

An analytical solution for the general dam–reservoir system described in the previous section is obtained for a problem with a simple geometry. As depicted in figure 2, the upstream dam face is assumed to be a straight line,

$$y = -x \tan \alpha\pi \quad \text{on } \Gamma_d. \tag{5}$$

The reservoir bottom is also a straight line and is described as

$$y = x \tan \beta\pi \quad \text{on } \Gamma_b, \tag{6}$$

where $0 < \alpha \leqslant \frac{1}{2}$ and $0 \leqslant \beta < \frac{1}{2}$. When $\beta = 0$, the reservoir depth becomes a constant and the reservoir domain extends to infinity ($x \to \infty$).

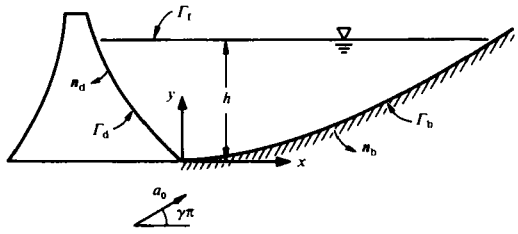

FIGURE 1. Schematic diagram of a dam–reservoir system.

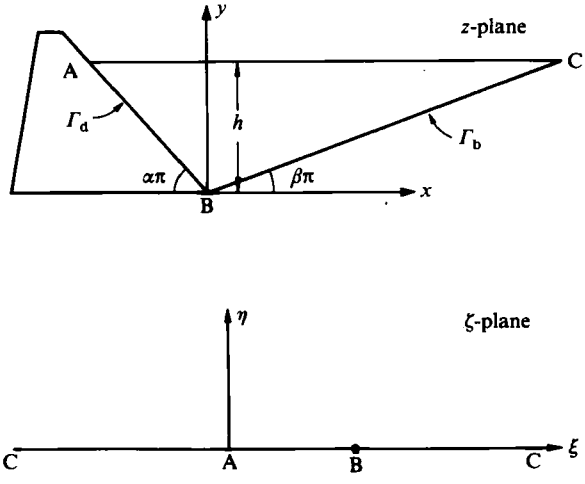

FIGURE 2. A simplified dam–reservoir system. The reservoir occupied by the water in the z-plane is mapped onto the upper half of the ζ-plane.

The boundary conditions along the solid surfaces can be reduced from (3), (4), (5) and (6) to

$$\frac{\partial P}{\partial n_d} = \rho a_0 \sin(\alpha+\gamma)\pi \quad \text{on } \Gamma_d, \tag{7}$$

$$\frac{\partial P}{\partial n_b} = \rho a_0 \sin(\beta-\gamma)\pi \quad \text{on } \Gamma_b. \tag{8}$$

Introducing the complex-conjugate function q with respect to P, we can construct an analytical function

$$W(z) = P+\mathrm{i}q, \quad z = x+\mathrm{i}y. \tag{9}$$

From the Cauchy–Riemann condition $\partial P/\partial n = \partial q/\partial s$, the boundary conditions (7) and (8) can be rewritten as

$$q = -\rho a_0 s \sin(\alpha+\gamma)\pi \quad \text{on } \Gamma_d, \tag{10}$$

$$q = -\rho a_0 \tilde{s} \sin(\beta-\gamma)\pi \quad \text{on } \Gamma_b, \tag{11}$$

where s measures the distance from the origin of a coordinate (point B in figure 2) to any point on the upstream dam face and $\tilde{s}$ represents the distance along the reservoir bottom measured from the origin.

Using the conformed mapping

$$z = K\int_1^{\zeta} t^{\alpha-1}(t-1)^{\delta-1}\,\mathrm{d}t; \quad \alpha+\beta+\delta = 1 \tag{12}$$

given by the Schwarz–Christoffel theory, we can transform the reservoir fluid region in the physical plane into the upper half of the ζ-plane ($\zeta = \xi + \mathrm{i}\eta$) (see figure 2). Points A and B are mapped into $\zeta = 0$ and 1 respectively. Point C is mapped into points at infinity in the ζ-plane along the negative and positive axes. The complex constant K in (12) determines the scale and the orientation of the triangle ABC in the z-plane and is given as

$$K = \mathrm{e}^{\mathrm{i}\pi\beta}\left(\frac{h\pi}{\sin\alpha\pi\,\sin\beta\pi}\right)\left(\frac{1}{\Gamma(\alpha)\,\Gamma(\beta)\,\Gamma(\delta)}\right), \tag{13}$$

where $\Gamma(\ )$ is the gamma function.

From (2), (9), (10) and (11), along the real axis in the ζ-plane, we have

$$\mathrm{Re}\,W(\zeta) = 0 \quad (-\infty < \xi < 0), \tag{14}$$

$$\mathrm{Im}\,W(\zeta) = \begin{cases} -\rho a_0\, s(\xi)\sin(\alpha+\gamma)\,\pi & (0 < \xi < 1), \quad (15)\\ -\rho a_0\,\tilde{s}(\xi)\sin(\beta-\gamma)\,\pi & (1 < \xi < \infty), \quad (16) \end{cases}$$

where s and $\tilde{s}$ are given in (12) as

$$s = K\,\mathrm{e}^{-\mathrm{i}\pi\beta}\int_{\xi}^{1} t^{\alpha-1}(1-t)^{\delta-1}\,\mathrm{d}t \quad (0 < \xi < 1) \tag{17}$$

and

$$\tilde{s} = K\,\mathrm{e}^{-\mathrm{i}\pi\beta}\int_1^{\xi} t^{\alpha-1}(t-1)^{\delta-1}\,\mathrm{d}t \quad (1 < \xi < \infty). \tag{18}$$

Note that $K\,\mathrm{e}^{-\mathrm{i}\pi\beta}$ is a real constant.

Equations (14), (15) and (16) are mixed boundary conditions for $W(\zeta)$. However, if we introduce an auxiliary function

$$H(\zeta) = \zeta^{-\frac{1}{2}}\,W(\zeta), \tag{19}$$

where the positive branch is taken for the square-root function, the boundary conditions become

$$\mathrm{Im}\,H(\zeta) = \begin{cases} 0 & (-\infty < \xi < 0), \quad (20)\\ -\rho a_0\,\xi^{-\frac{1}{2}}\,s(\xi)\sin(\alpha+\gamma)\,\pi & (0 < \xi < 1), \quad (21)\\ -\rho a_0\,\xi^{-\frac{1}{2}}\,\tilde{s}(\xi)\sin(\beta-\gamma)\,\pi & (1 < \xi < \infty). \quad (22) \end{cases}$$

Using the Riemann–Hilbert theorem (e.g. Carrier, Krook & Pearson 1966), we can express the analytic function $H(\zeta)$ in the upper-half ζ-plane as

$$H(\zeta) = \frac{1}{\pi}\int_{-\infty}^{\infty} \frac{\mathrm{Im}\,H(\xi)\,\mathrm{d}\xi}{\xi-\zeta}. \tag{23}$$

Substitutions of (20), (21) and (22) into (23) yield

$$W(\zeta) = -\frac{\rho a_0}{\pi}\,\zeta^{\frac{1}{2}}\left\{\sin(\alpha+\gamma)\,\pi\int_0^1 \frac{s(\xi)\,\mathrm{d}\xi}{\xi^{\frac{1}{2}}(\xi-\zeta)} + \sin(\beta-\gamma)\,\pi\int_1^{\infty}\frac{\tilde{s}(\xi)\,\mathrm{d}\xi}{\xi^{\frac{1}{2}}(\xi-\zeta)}\right\}. \tag{24}$$

The hydrodynamic pressure on the upstream dam face is the real part of $W(\zeta)$ for $0 < \xi < 1$. Using (17) and (18) in (24) and integrating by parts, we have

$$P(\xi) = \frac{K\,\mathrm{e}^{-\mathrm{i}\pi\beta}}{\pi}\rho a_0\left\{\sin(\alpha+\gamma)\pi \int_0^1 t^{\alpha-1}(1-t)^{\delta-1}\ln\left|\frac{t^{\frac{1}{2}}+\zeta^{\frac{1}{2}}}{t^{\frac{1}{2}}-\zeta^{\frac{1}{2}}}\right|\mathrm{d}t\right.$$
$$\left. -\sin(\beta-\gamma)\pi \int_1^\infty t^{\alpha-1}(t-1)^{\delta-1}\ln\left|\frac{t^{\frac{1}{2}}+\zeta^{\frac{1}{2}}}{t^{\frac{1}{2}}-\zeta^{\frac{1}{2}}}\right|\mathrm{d}t\right\} \quad (0<\xi<1), \quad (25)$$

where $\int$ denotes the Cauchy principal value. For computational purposes the above equation can be expressed in a different form. Differentiating (25) with respect to ξ, we obtain

$$\frac{\mathrm{d}P(\xi)}{\mathrm{d}\xi} = \frac{K\,\mathrm{e}^{-\mathrm{i}\pi\beta}}{\pi\xi^{\frac{1}{2}}}\rho a_0\left\{\sin(\alpha+\gamma)\,\pi \int_0^1 t^{\alpha-1}(1-t)^{\delta-1}\frac{t^{\frac{1}{2}}}{(t-\xi)}\,\mathrm{d}t\right.$$
$$\left. -\sin(\beta-\gamma)\pi \int_1^\infty t^{\alpha-1}(t-1)^{\delta-1}\frac{t^{\frac{1}{2}}}{(t-\xi)}\,\mathrm{d}t\right\} \quad (0<\xi<1). \quad (26)$$

The integrals on the right-hand side of (26) can be obtained by contour integrations (see Appendix). Thus

$$\frac{\mathrm{d}P(\xi)}{\mathrm{d}\xi} = \frac{K\,\mathrm{e}^{-\mathrm{i}\pi\beta}}{\pi\xi^{\frac{1}{2}}}\rho a_0\left\{\frac{[\sin(\alpha+\gamma)\pi\cos\beta\pi+\sin(\beta-\gamma)\pi\cos\alpha\pi]}{\sin[(\alpha+\beta)\pi]}\int_0^\infty \frac{t^\alpha}{(1+t)^{1-\delta}}\frac{\mathrm{d}t}{t^{\frac{1}{2}}(t+\xi)}\right.$$
$$\left. -\frac{\pi[\sin(\alpha+\gamma)\pi\cos(\alpha+\beta)\pi+\sin(\beta-\gamma)\pi]}{\sin(\alpha+\beta)\pi}\frac{\xi^\alpha}{(1-\xi)^{1-\delta}}\frac{1}{\xi^{\frac{1}{2}}}\right\} \quad (0<\xi<1). \quad (27)$$

Integrating (27), we have

$$P(\xi) = \frac{K\,\mathrm{e}^{-\mathrm{i}\pi\beta}}{\pi}\rho a_0\left\{\frac{4[\sin(\alpha+\gamma)\pi\cos\beta\pi+\sin(\beta-\gamma)\pi\cos\alpha\pi]}{\sin[(\alpha+\beta)\pi]}\right.$$
$$\left.\times\int_0^{\frac{1}{2}\pi}\frac{\xi^\alpha}{(\tan^2\theta+\xi)^{1-\delta}}\frac{(\tan\theta)^{2\beta}\theta\,\mathrm{d}\theta}{\sin\theta\cos\theta}\right\}$$
$$-\rho a_0\frac{\sin(\alpha+\gamma)\pi\cos(\alpha+\beta)\pi+\sin(\beta-\gamma)\pi}{\sin(\alpha+\beta)\pi}\left[\frac{h}{\sin\alpha\pi}-s(\xi)\right] \quad (0<\xi<1). \quad (28)$$

We remark here that the analytical solutions presented by Chwang (1978, 1979) are the special cases of (28) with $\beta = \gamma = 0$ and $\alpha = \frac{1}{2}$ respectively.

3.2. *Solutions and discussion*

Using (18) and (28), hydrodynamic pressures are only calculated for horizontal ground acceleration (i.e. $\gamma = 0°$). The vertical ground acceleration simply modifies the gravitational acceleration. Therefore, the corresponding hydrodynamic pressure varies linearly in the vertical direction independently of the geometries of reservoir and dam (Chwang 1979).

The hydrodynamic pressure distributions on the upstream dam face are plotted *vs* the vertical distance y/h for several bottom slopes $\beta\pi$ between 0° and 90° in figures 3–6. In each figure hydrodynamic pressures for several inclination angles $\alpha\pi$ are presented. When the water depth becomes a constant in the reservoir ($\beta\pi = 0$), the present theory reduces to Chwang's (1978) solution. Moreover, the hydrodynamic pressures for the vertical upstream dam face ($\alpha\pi = 90°$) agree with Chwang's (1979) results. In figure 3 Zangar's (1953) laboratory data obtained by using an electrical

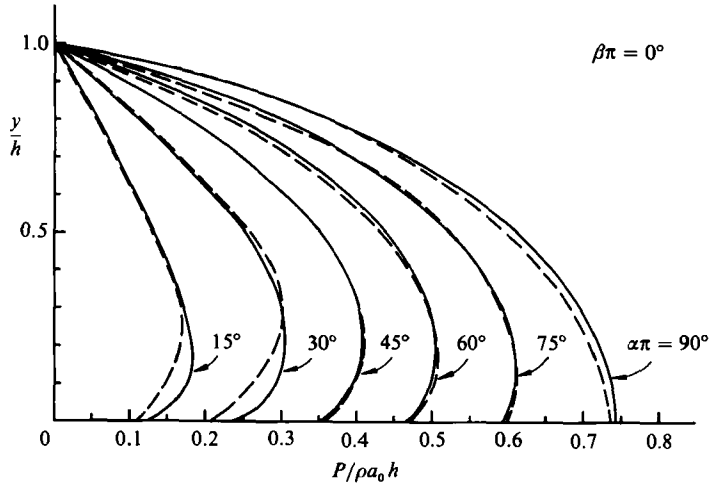

FIGURE 3. The pressure distributions on the upstream dam face when the water depth is constant in the reservoir; ——, present theory; – – –, Zangar's (1953) experimental results.

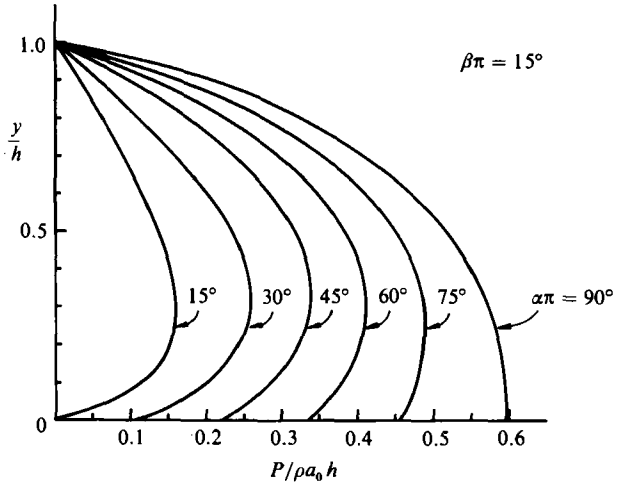

FIGURE 4. The pressure distributions on the upstream dam face for different bottom slopes.

analogue are also plotted. The agreement between the theory and the experimental data is fairly good. The experimental data seem to underpredict the pressures near the bottom of the reservoir when the inclination angles are relatively small, i.e. $\alpha\pi = 15°$ and $30°$. From figures 3–6 it is clear that the hydrodynamic pressure decreases as $\beta\pi$ increases, whereas the pressure increases as $\alpha\pi$ increases. Therefore, the pressure distribution for $\alpha\pi = 90°$ (vertical upstream dam face) and $\beta = 0°$ (constant water depth) is the maximum envelope of all pressure distributions. Regardless of the bottom slope of the reservoir, the maximum pressure always occurs at the base of the dam when the upstream dam face is vertical. For different angles of upstream dam-face inclination, maximum pressure occurs at some distance above the base of the dam. In fact, the theory shows that negative hydrodynamic pressure appears near the base of the dam when the inclination angle is relatively small and the bottom slope is relatively large.

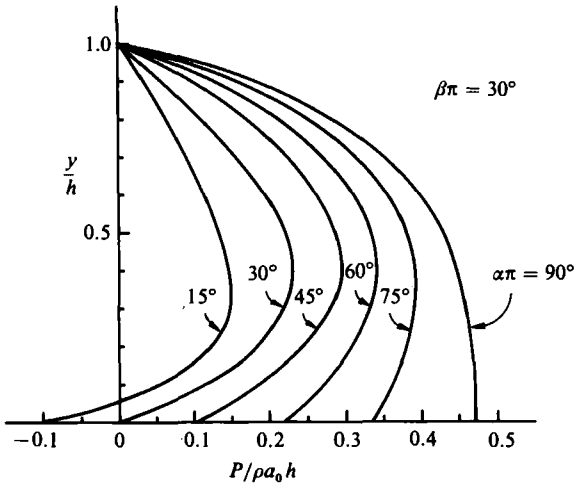

FIGURE 5. The pressure distributions on the upstream dam face for different bottom slopes.

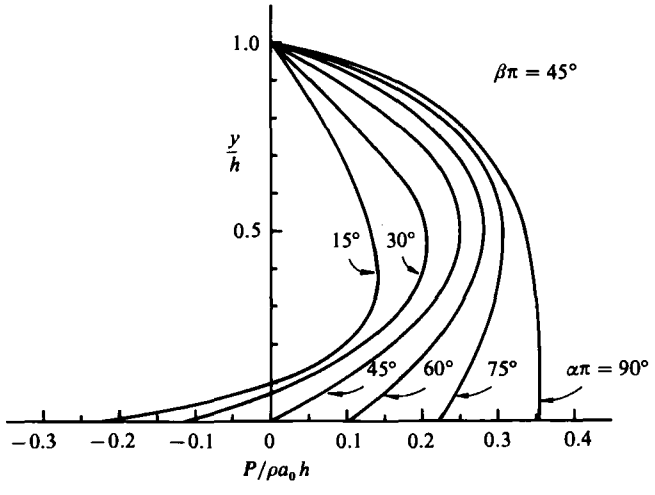

FIGURE 6. The pressure distributions on the upstream dam face for different bottom slopes.

Chwang (1979) has pointed out the possibility of cavitation on the dam face when the dam is accelerating in the negative x-direction. The possibility of cavitation is enhanced if the dam is also accelerating in the negative y-direction. The locations of cavitation are usually very close to the top of the dam. In the present cases where the upstream dam surface is not vertical, the hydrodynamic pressure becomes negative near the toe of the dam (e.g. figures 5 and 6). Although the negative pressure is perhaps too small to cause cavitation by itself for a realistic earthquake intensity, a combination of vertical acceleration in the negative y-direction and horizontal acceleration in the positive x-direction could create cavitation near the toe of the dam face.

4. An integral-equation method

4.1. *Theoretical formulation*

The analytical solution presented in the previous section is limited to simple geometries where the slopes of the upstream face and the reservoir bottom are constants. For dam–reservoir systems with more complex geometries, solutions to the boundary-value problem described by (1)–(4) must be obtained by numerical means. Many numerical methods, such as the finite-element and the finite-differences methods, are readily available to solve the problem. However, since only the hydrodynamic pressures on the dam surface are of interest, an integral-equation method involving only the boundary variables would be more efficient. This method has been developed extensively in the literature (e.g. Liggett & Liu 1983). Only a brief outline of the method is given below.

Referring to figure 1, the boundary of the computational domain Γ consists of the free surface Γ_f, the rigid bottom Γ_b, and the upstream dam face Γ_d. Applying the Green's second identity to P and the free-space Green's function of the Laplace equation G one can obtain the following integral equation:

$$\left.\begin{aligned} \alpha P(x, y) = \int_\Gamma \left[P(x', y') \frac{\partial G}{\partial n} - G \frac{\partial P(x', y')}{\partial n} \right] \mathrm{d}s(x', y'), \\ \Gamma = \Gamma_f \cup \Gamma_b \cup \Gamma_d, \end{aligned}\right\} \tag{29}$$

where $\alpha = 0$ if (x, y) is outside of the computational domain and $\alpha = 1$ if (x, y) is an interior point. But, when (x, y) is a boundary point, α takes the value of the interior angle of the boundary at that point divided by 2π. Hence, if the boundary is smooth, the interior angle is π and α is $\frac{1}{2}$. The free-space Green's function of the Laplace equation, corresponding to a point source at (x, y), is given as

$$G(x', y'; x, y) = \ln r; \quad r = [(x-x')^2 + (y-y')^2]^{\frac{1}{2}}. \tag{30}$$

If the source point (x, y) is located on the boundary, (29) is an integral equation which can be solved for missing information along the boundary. Substituting boundary conditions (2)–(4) into (29), we have

$$\alpha P + \int_{\Gamma_f} \frac{\partial P}{\partial n_f} \mathrm{d}s - \int_{\Gamma_b} P \frac{\partial G}{\partial n_b} \mathrm{d}s - \int_{\Gamma_d} P \frac{\partial G}{\partial n_d} \mathrm{d}s = \rho \int_{\Gamma_b} \boldsymbol{a} \cdot \boldsymbol{n}_b \, G \, \mathrm{d}s + \rho \int_{\Gamma_d} \boldsymbol{a} \cdot \boldsymbol{n}_d \, G \, \mathrm{d}s. \tag{31}$$

The right-hand side of the above equation contains the known boundary conditions and the left-hand side involves the unknown P or $\partial P/\partial n$ along each segment of the boundary. Various methods for discretizing the above equation numerically have been reviewed in many papers (e.g. Liggett & Liu 1983) and will not be repeated here. Linear elements with linear interpolation functions for P and $\partial P/\partial n$ on each element are used in this paper.

When the horizontal dimension of the reservoir is much larger than the water depth, the computational domain must be truncated and a fictitious boundary should be inserted at some distance away from the dam so that the hydrodynamic pressures are indeed negligible along the fictitious boundary. Therefore, the location of the fictitious boundary is determined, to a large extent, by the trial-and-error method. A more elegant hybrid technique similar to that developed by Mei, Foda & Tong (1979) is outlined in the following section.

We consider a reservoir which extends to infinity ($x \to \infty$). As shown in figure 7,

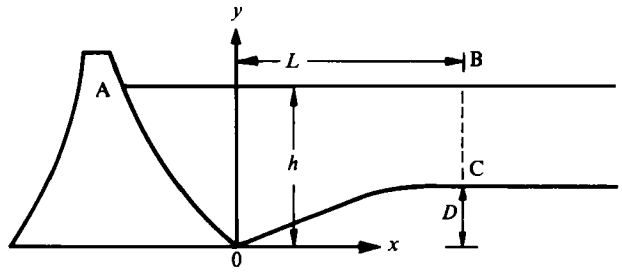

FIGURE 7. Schematic diagram of a dam–reservoir system with a fictitious boundary.

the fictitious boundary is represented by BC ($x = L$). We assume that the water depth becomes a constant beyond the fictitious boundary. If only the horizontal ground acceleration is considered, the analytical solution in the region $x > L$ can be readily expressed as

$$P = \sum_{n=1}^{\infty} A_n \cos k_n(y-D)\, \mathrm{e}^{-k_n x} \quad (x \geqslant L), \tag{32}$$

$$k_n = \frac{n\pi}{2(h-D)} \quad (n = 1, 2, 3, \ldots), \tag{33}$$

where A_n ($n = 1, 2, 3, \ldots$) are unknown constants. It is clear that (32) satisfies the Laplace equation and the boundary conditions including the zero-pressure condition at infinity. The normal derivative of the pressure along the fictitious boundary can be obtained from (32):

$$\frac{\partial P}{\partial n} = \frac{\partial P}{\partial x} = -\sum_{n=1}^{\infty} A_n k_n \cos k_n(y-D)\, \mathrm{e}^{-k_n L}. \tag{34}$$

The integral equation for this problem remains the same as (29) with an additional integral over the fictitious boundary. Equations (32) and (34) are used in the integrand to replace P and $\partial P/\partial n$ by a set of unknown coefficients A_n. The series in (32) and (34) must be truncated to have the same number of unknown coefficients as the number of nodal points on the fictitious boundary.

4.2. *Numerical solutions and discussion*

To demonstrate the applicability of the integral-equation method for problems with complex geometries, numerical solutions are obtained for several different shapes of dams as shown in figure 8. The reservoir has a constant depth and extends to infinity, $x \to \infty$. Using an electrical analogue, Zangar (1953) obtained experimental data of hydrodynamic pressures on dam faces of the same geometries.

In our numerical computations, a fictitious boundary is located at $x = L = 6h$. A total of forty-three nodal points are used to discretize the entire boundary. These nodal points are more or less evenly distributed. Only two terms in the series of (32) and (34) are used in the computations.

Numerical solutions as well as Zangar's experimental data are plotted in figure 9. Our numerical solutions for the vertical-dam case (B5; $\alpha\pi = 90°$) and the constant-slope case (B1; $\alpha\pi = 60°$) agree almost perfectly with the analytical solutions presented in §3. The slight differences between Zangar's data and the theoretical solution have been shown in figure 3. Agreement between numerical solutions and experimental data is also fairly good for other shapes of dams with the exception of

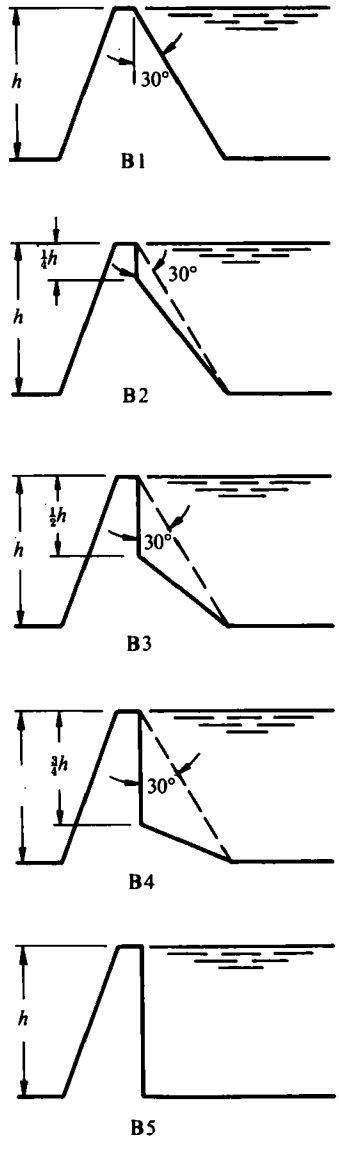

FIGURE 8. Five different shapes for the upstream face of dam.

the B3 case. In that case the vertical portion of the dam face extends to one-half of the water depth. Experimental data indicated larger hydrodynamic pressures than predicted by the theory. The hydrodynamic-pressure distribution for the vertical-dam case serves as an envelope (maximum bound) for all other pressure profiles.

5. Concluding remarks

Analytical solutions are obtained for the hydrodynamic pressure on an accelerating rigid dam. The reservoir is allowed to have a triangular shape. A numerical scheme *via* the integral-equation method is also developed to treat problems with complex geometries. The theory is developed based on the simplifying assumption that the

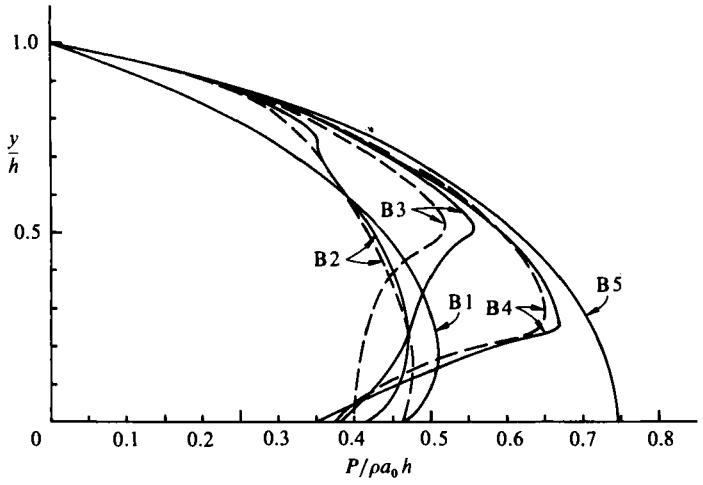

FIGURE 9. The pressure distributions on the upstream face of dam for the shapes shown in figure 8; ——, present theory; – – –, Zangar's (1953) data.

compressibility of water can be neglected. This assumption is valid as long as the fluid-particle velocity in the reservoir V_f is small in comparison with the speed of sound in the water, V_s. The ground acceleration a_0 during a typical earthquake ranges from $0.1g$ to $1.0g$, and the period of the ground excitation T varies from 0.1 s to 10 s. The ratio V_f/V_s ranges from 10^{-1} to 10^{-4}.

It is found that, regardless of the bottom slope of the reservoir, the maximum pressure always occurs at the base of the dam when the upstream dam face is vertical. Moreover, the negative hydrodynamic pressure appears near the toe of the dam when the inclination angle is small and the bottom slope is large. The appearance of the negative pressure could create cavitations.

This research was supported, in part, by a research grant, sponsored by the National Science Foundation (CEE-7902803 A04), to Cornell University. Discussions with Dr Allen T. Chwang have been most useful. His effort and time are much appreciated.

Appendix. Contour integrations for (26)

Let is denote the integrals on the right-hand side of (26) by

$$I_1 = \int_0^1 t^{\alpha-1}(1-t)^{\delta-1}\frac{t^{\frac{1}{2}}}{t-\xi}\,\mathrm{d}t, \tag{A 1}$$

$$I_2 = \int_1^\infty t^{\alpha-1}(t-1)^{\delta-1}\frac{t^{\frac{1}{2}}}{t-\xi}\,\mathrm{d}t. \tag{A 2}$$

The integrands in I_1 and I_2 have three branch points in the complex t-plane, $t = 0, +1$ and ∞. Both integrals can be integrated by contour integrations.

The contour and branch cuts for I_1 are shown in figure 10. The phase of t and $(t-1)$ is between $-\pi$ and π. There is a simple pole at $t = \xi$. The contour integral is composed of the following integrals:

$$\int_C t^{\alpha-1}(t-1)^{\delta-1}\frac{t^{\frac{1}{2}}}{t-\xi}\,\mathrm{d}t = \int_{C_R} + \int_{-\infty}^0 + \int_0^1 + \int_1^0 + \int_0^{-\infty} + \int_{C_\epsilon},$$

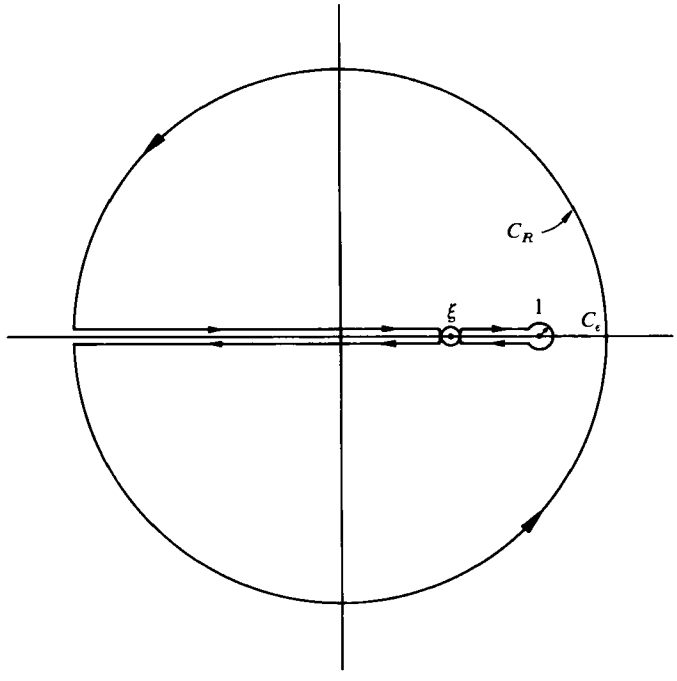

FIGURE 10. Contours and branch cuts for I_1 (A 1).

where C_R is a circle of large radius R and C_ϵ represents a small circle of radius ϵ centred at $t = 1$. The integral around C_R vanishes as R approaches infinity, as does that around C_ϵ as $\epsilon \to 0$. The remaining integrals can be written as

$$\int_{-\infty}^{0} t^{\alpha-1}(t-1)^{\delta-1}\frac{t^{\frac{1}{2}}}{t-\xi}\,\mathrm{d}t = \int_{-\infty}^{0} \frac{|t|^{\alpha-1}|1-t|^{\delta-1}\,\mathrm{e}^{\mathrm{i}(\alpha+\delta-2)\pi}|t|^{\frac{1}{2}}\,\mathrm{e}^{\frac{1}{2}\mathrm{i}\pi}\,\mathrm{d}t}{t-\xi}$$

$$= \mathrm{i}\,\mathrm{e}^{-\mathrm{i}\beta\pi}\int_0^\infty \frac{t^\alpha}{(t+1)^{1-\delta}}\frac{\mathrm{d}t}{t^{\frac{1}{2}}(t+\xi)}, \tag{A 3}$$

$$\int_0^1 t^{\alpha-1}(t-1)^{\delta-1}\frac{t^{\frac{1}{2}}}{t-\xi}\,\mathrm{d}t = \mathrm{e}^{\mathrm{i}(\delta-1)\pi}\int_0^1 \frac{t^\alpha}{(1-t)^{1-\delta}}\frac{\mathrm{d}t}{t^{\frac{1}{2}}(t-\xi)}, \tag{A 4}$$

$$\int_1^0 t^{\alpha-1}(t-1)^{\delta-1}\frac{t^{\frac{1}{2}}}{t-\xi}\,\mathrm{d}t = -\mathrm{e}^{-\mathrm{i}(\delta-1)\pi}\int_0^1 \frac{t^\alpha}{(1-t)^{1-\delta}}\frac{\mathrm{d}t}{t^{\frac{1}{2}}(t-\xi)}, \tag{A 5}$$

$$\int_0^{-\infty} t^{\alpha-1}(t-1)^{\delta-1}\frac{t^{\frac{1}{2}}}{t-\xi}\,\mathrm{d}t = \int_{-\infty}^{0} \frac{|t|^{\alpha-1}|1-t|^{\delta-1}\,\mathrm{e}^{\mathrm{i}(\alpha+\delta-2)\pi}|t|^{\frac{1}{2}}\,\mathrm{e}^{\frac{1}{2}\mathrm{i}\pi}\,\mathrm{d}t}{t-\xi}$$

$$= \mathrm{i}\,\mathrm{e}^{\mathrm{i}\beta\pi}\int_0^\infty \frac{t}{(t+1)^{1-\delta}}\frac{\mathrm{d}t}{t^{\frac{1}{2}}(t+\xi)}. \tag{A 6}$$

The contour integral is equal to the residue at the simple pole $t = \xi$, which can be evaluated as

$$\mathrm{Res}\,(t=\xi) = \pi\mathrm{i}\,\frac{\xi^\alpha}{(1-\xi)^{1-\delta}}\frac{1}{\xi^{\frac{1}{2}}}\,\mathrm{e}^{\mathrm{i}(\delta-1)\pi} + \pi\mathrm{i}\,\frac{\xi^\alpha}{(1-\xi)^{1-\delta}}\frac{1}{\xi^{\frac{1}{2}}}\,\mathrm{e}^{-\mathrm{i}(\delta-1)\pi}$$

$$= 2\pi\mathrm{i}\cos[(\alpha+\beta)\pi]\,\frac{\xi^\alpha}{(1-\xi)^{1-\delta}}\frac{1}{\xi^{\frac{1}{2}}}. \tag{A 7}$$

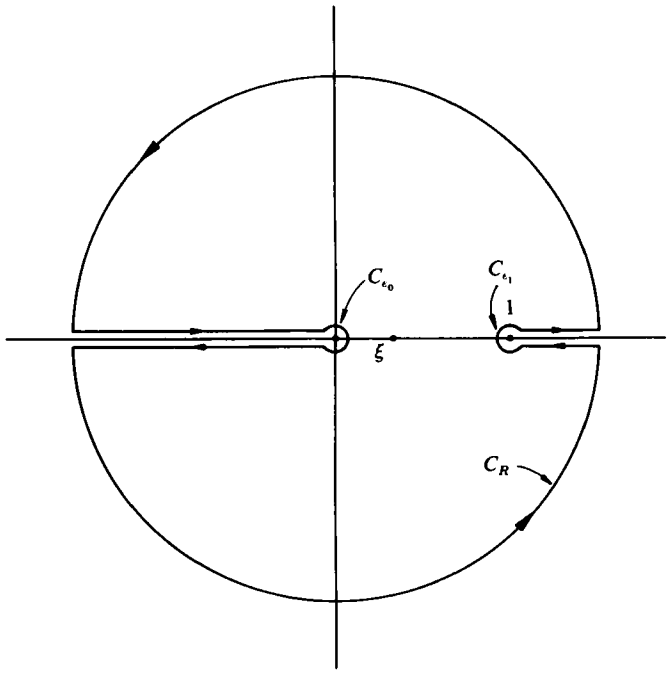

FIGURE 11. Contours and branch cuts for I_2 (A 2).

Thus
$$\int_C t^{\alpha-1}(t-1)^{\delta-1}\frac{t^{\frac{1}{2}}}{t-\xi}\,\mathrm{d}t = \mathrm{Res}\,(t=\xi).$$

Substituting (A 3)–(A 7) into the above equation, we obtain

$$I_1 = \int_0^1 \frac{t^\alpha}{(1-t)^{1-\delta}}\frac{\mathrm{d}t}{t^{\frac{1}{2}}(t-\xi)} = \frac{\cos\beta\pi}{\sin[(\alpha+\beta)\pi]}\int_0^\infty \frac{t^\alpha}{(1+t)^{1-\delta}}\frac{\mathrm{d}t}{t^{\frac{1}{2}}(t+\xi)}$$
$$-\frac{\pi\cos[(\alpha+\beta)\pi]}{\sin[(\alpha+\beta)\pi]}\frac{\xi^\alpha}{(1-\xi)^{1-\delta}}\frac{1}{\xi^{\frac{1}{2}}}. \quad \text{(A 8)}$$

For I_2 in (A 2), the contour and the branch cuts are shown in figure 11. The phase of t is between $-\pi$ and π, but the range of the phase of $(t-1)$ is from 0 to 2π. The contour integral becomes

$$\int_C t^{\alpha-1}(t-1)^{\delta-1}\frac{t^{\frac{1}{2}}}{t-\xi}\,\mathrm{d}t = \int_{C_R}+\int_{C_{\epsilon_1}}+\int_{C_{\epsilon_0}}+\int_{-\infty}^0+\int_0^{-\infty}+\int_\infty^1+\int_1^\infty,$$

where C_{ϵ_0} and C_{ϵ_1} denote small circles with radius ϵ_0 and ϵ_1 centred at $t=0$ and 1 respectively (see figure 11). Once again, the integral around the large circle C_R vanishes as $R\to\infty$. The integrals around C_{ϵ_0} and C_{ϵ_1} also become zero as ϵ_0 and $\epsilon_1\to 0$. Using the proper phase of t and $(t-1)$, we find the remaining integrals in the above equation to be expressed as

$$\int_{-\infty}^0 \frac{t^{\alpha-1}(t-1)^{\delta-1}t^{\frac{1}{2}}}{t-\xi}\,\mathrm{d}t = \int_{-\infty}^0 \frac{|t|^{\alpha-1}|t-1|^{\delta-1}\,\mathrm{e}^{\mathrm{i}\pi(\alpha+\delta-2)}|t|^{\frac{1}{2}}\,\mathrm{e}^{\frac{1}{2}\mathrm{i}\pi}}{t-\xi}\,\mathrm{d}t$$
$$= -\mathrm{i}\,\mathrm{e}^{-\mathrm{i}(\beta+1)\pi}\int_0^\infty \frac{t^\alpha}{(1+t)^{1-\delta}}\frac{\mathrm{d}t}{t^{\frac{1}{2}}(t+\xi)}, \quad \text{(A 9)}$$

$$\int_0^{-\infty} \frac{t^{\alpha-1}(t-1)^{\delta-1}t^{\frac{1}{2}}}{t-\xi}\,\mathrm{d}t = \int_0^{-\infty} \frac{|t|^{\alpha-1}|t-1|^{\delta-1}\,\mathrm{e}^{\mathrm{i}(\delta-\alpha)\pi}|t|^{\frac{1}{2}}\,\mathrm{e}^{-\frac{1}{2}\mathrm{i}\pi}}{t-\xi}\,\mathrm{d}t$$

$$= -\mathrm{i}\,\mathrm{e}^{\mathrm{i}(\delta-\alpha)\pi}\int_0^{\infty} \frac{t^{\alpha}}{(1+t)^{1-\delta}}\frac{\mathrm{d}t}{t^{\frac{1}{2}}(t+\xi)}, \tag{A 10}$$

$$\int_1^{\infty} \frac{t^{\alpha-1}(t-1)^{\delta-1}t^{\frac{1}{2}}}{t-\xi}\,\mathrm{d}t = \int_1^{\infty} \frac{t^{\alpha}}{(t-1)^{1-\delta}}\frac{\mathrm{d}t}{t^{\frac{1}{2}}(t-\xi)}, \tag{A 11}$$

$$\int_{\infty}^1 \frac{t^{\alpha-1}(t-1)^{\delta-1}t^{\frac{1}{2}}}{t-\xi}\,\mathrm{d}t = \int_{\infty}^1 \frac{t^{\alpha-1}(t-1)^{\delta-1}\,\mathrm{e}^{2\mathrm{i}(\delta-1)\pi}t^{\frac{1}{2}}}{t-\xi}\,\mathrm{d}t$$

$$= -\mathrm{e}^{-2\mathrm{i}(\alpha+\beta)\pi}\int_1^{\infty} \frac{t^{\alpha}}{(t-1)^{1-\delta}}\frac{\mathrm{d}t}{t^{\frac{1}{2}}(t-\xi)}. \tag{A 12}$$

The residue of the contour integral is contributed by the simple pole at $t = \xi$,

$$\mathrm{Res}\,(t=\xi) = 2\pi\mathrm{i}\,\xi^{\alpha-1}\xi^{\frac{1}{2}}|\xi-1|^{\delta-1}\,\mathrm{e}^{\mathrm{i}(\delta-1)\pi}$$

$$= -2\pi\mathrm{i}\,\xi^{\alpha-1}(1-\xi)^{\delta-1}\xi^{\frac{1}{2}}\,\mathrm{e}^{\mathrm{i}\delta\pi}. \tag{A 13}$$

Applying the residue theorem with (A 9)–(A 13) we obtain

$$I_2 = \int_1^{\infty} t^{\alpha-1}(t-1)^{\delta-1}\frac{t^{\frac{1}{2}}}{t-\xi}\,\mathrm{d}t = \frac{\pi\xi^{\alpha}}{\sin\delta\pi\,(1-\xi)^{1-\delta}\,\xi^{\frac{1}{2}}} - \frac{\cos\alpha\pi}{\sin\delta\pi}\int_0^{\infty} \frac{t^{\alpha}\,\mathrm{d}t}{(1+t)^{1-\delta}\,t^{\frac{1}{2}}(t+\xi)}. \tag{A 14}$$

REFERENCES

Carrier, G. F., Krook, M. & Pearson, C. E. 1966 *Function of a Complex Variable.* McGraw-Hill.

Chopra, A. K. 1967 Hydrodynamic pressures on dams during earthquakes. *J. Engng Mech. Div. ASCE* **93**, 205–223.

Chwang, A. T. 1978 Hydrodynamic pressures on sloping dams during earthquakes. Part 2. Exact theory. *J. Fluid Mech.* **87**, 343–348.

Chwang, A. T. 1979 Hydrodynamic pressure on an accelerating dam and criteria for cavitation. *J. Engng Maths* **13**, 143–152.

Chwang, A. T. 1981 Effect of stratification on hydrodynamic pressures on dams. *J. Engng Maths* **15**, 49–63.

Chwang, A. T. & Housner, G. W. 1978 Hydrodynamic pressures on sloping dams during earthquakes. Part 1. Momentum method. *J. Fluid Mech.* **87**, 335–341.

Fenves, G. & Chopra, A. K. 1983 Effects of reservoir bottom absorption on earthquake response of concrete gravity dam. *J. Earthquake Engng and Structural Dynamics* **11**, 809–829.

Fenves, G. & Chopra, A. K. 1985 Effects of reservoir bottom absorption and dam–water–foundation rock interaction on frequency response function for concrete gravity dams. *J. Earthquake Engng and Structural Dynamics* **13**, 13–32.

Finn, W. D. L. & Varoglu, E. 1973 Dynamics of gravity dam–reservoir systems. *Computers Struct.* **3**, 913–924.

Hall, J. F. & Chopra, A. K. 1982 Two-dimensional dynamic analysis of concrete gravity and embankment dams including hydrodynamic effects. *J. Earthquake Engng and Structural Dynamics* **10**, 305–332.

Kármán, T. von 1933 Discussion of water pressures on dams during earthquakes. *Trans. ASCE* **98**, 434–436.

Liggett, J. A. & Liu, P. L.-F. 1983 *Boundary Integral Equation Method Applied to Flow in Porous Media.* George Allen and Unwin.

Liu, P. L.-F. & Cheng, A. H.-D. 1984 Boundary solution for fluid–structure interaction. *J. Hydraulic Engng, ASCE* **110**, 51–64.

MEI, C. C., FODA, M. A. & TONG, P. 1979 Exact and hybrid-element solutions for the vibration of a thin elastic structure seated on the sea floor. *Applied Ocean Research* **1**, 79–88.

RASHED, A. A. & IWAN, W. D. 1984 Earthquake response of short-length gravity dams. In *Proc. 8th World Conf. on Earthquake Engineering*, San Francisco, California, VII, pp. 343–350.

RASHED, A. A. 1982 Dynamic analysis of fluid–structure systems. *Rep. No. EERL* 82-03, Earthquake Engineering Research Laboratory, California Institute of Technology, Pasadena, California.

WESTERGAARD, H. M. 1933 Water pressures on dams during earthquakes. *Trans. ASCE* **98**, 418–433.

YEH, C.-S. & HO, Y.-C. 1984 Earthquake induced water pressures on a gravity dam from a reservoir with inclined basin. In *Proc. CCNAA-AIT Joint Seminar on Multiple Hazards Mitigation*, Tainan, Taiwan, 107–133.

ZANGAR, C. N. 1953 Hydrodynamic pressures on dams due to horizontal earthquakes. *Proc. Soc. Exp. Stress Anal.* **10**, 93–102.